



Experimental and simulation study of the effect of surface functional groups decoration on CH₄ and H₂ storage capacity of microporous carbons

Shohreh Mirzaei^a, Ali Ahmadpour^{a,*}, Akbar Shahsavand^a, Ali Nakhaei Pour^b, Leila LotfiKatooli^c, Ali Garmroodi Asil^d, Babak Pouladi^e, Arash Arami-Niya^{f,*}

^a Department of Chemical Engineering, Faculty of Engineering, Ferdowsi University of Mashhad, P.O. Box 91779-48944, Mashhad, Iran

^b Department of Chemistry, Faculty of Science, Ferdowsi University of Mashhad, Mashhad, Iran

^c Department of Chemical Engineering, Faculty of Engineering, Golestan University, Gorgan, Iran

^d Department of Chemical Engineering, Faculty of Engineering, University of Bojnord, Bojnord, Iran

^e Research and Development Department (R&D), South Pars Gas Complex (SPGC), Asaluyeh, Bushehr, Iran

^f Discipline of Chemical Engineering, Western Australian School of Mines: Minerals, Energy and Chemical Engineering, Curtin University, GPO Box U1987, Perth, WA 6845, Australia

ARTICLE INFO

Keywords:

Activated carbon
Methane
Hydrogen
Gas storage
Adsorption
Heteroatoms
DFT
GCMC

ABSTRACT

The incorporation of heteroatoms (i.e. N, O, S, F) into the microporous carbon framework is proposed to affect the interactions between adsorbates and adsorbents and improve the efficiency of gas storage. We demonstrate a facile synthesis of coal-derived activated carbons (ACs) modified with oxygen and nitrogen-containing groups for CH₄ and H₂ storage application. The functionalised ACs showed to have a high surface area of 1617–1924 m²/g, and pore volume of 0.85–0.92 cm³/g. The AC samples prepared by pre-oxidation followed by amination possess comparatively high CH₄ adsorption capacity of 13.8 to 14.2 mmol/g at 298 K and 40 bar. However, the pristine AC and the oxidised AC showed the maximum H₂ adsorption capacity with 0.6 mmol/g and 0.44 mmol/g, respectively, at 20 bar and 298 K. Density functional theory (DFT) calculations were performed to study the adsorption of CH₄ and H₂ on the ACs with/without the surface functional groups. In agreement with the experimental results, the computational analysis showed an increase in the gas–solid interaction after surface modification. Finally, a well-known method of Grand Canonical Monte Carlo (GCMC) was used to simulate the studied gas adsorption systems and calculate the adsorption isotherms of CH₄ and H₂ on different ACs.

1. Introduction

Methane (CH₄) and hydrogen (H₂) counted as favourable fuels due to the production of a higher value of energy content per mass with minimal environmental impacts [1,2]. A considerable obstacle in the application of these energy carriers as an automotive fuel is their relatively low energy density [3]. Although two conventional methods of liquefaction and compression have been utilised to store these gaseous energy carriers, these methods are associated with the disadvantages of expensive investment costs and challenging operating conditions (high pressure or cryogenic temperature). To overcome these imperfections, the adsorption of CH₄ and H₂ in solid-state materials is currently attracting a great deal of attention [3,4]. Among different types of porous materials for gas storage application, carbon-based adsorbents are one of the most cost-effective and available materials which have strong thermal stability and high range of specific surface area (500–3800 m²/

g) [1].

Besides the direct effect of carbon's microporosity on the gas storage capacity [5–11], it is crucial to incorporate the role of structural heteroatoms (i.e. N, O, S, F) on the efficiency of gas storage [2,12]. The modification of solid's surface chemistry can improve the adsorbent-adsorbate interaction and results in a higher gas adsorption capacity, especially in the case of CH₄ and H₂ [2,13–20]. According to Im *et al.*, the CH₄ adsorption in electrospun carbon fibres increased up to 18.1 wt % (defined as the ratio of the mass of stored gas to the total mass of the storage system) after introducing fluorine to the carbon surface [18]. They have suggested that the non-polar structure of CH₄ molecules near carbon pores will be affected by the high electronegativity of fluorine, which results in grabbing effects and higher uptake of CH₄ molecules. Xia *et al.* studied the influence of nitrogen doping on the H₂ uptake and storage capacity of high surface area carbon materials and reported an increase of 4.1 and 6.9 wt% in the H₂ absorption of the adsorbents after

* Corresponding authors.

E-mail addresses: Ahmadpour@um.ac.ir (A. Ahmadpour), Arash.araminiya@curtin.edu.au (A. Arami-Niya).

<https://doi.org/10.1016/j.apsusc.2020.147487>

Received 28 April 2020; Received in revised form 6 August 2020; Accepted 6 August 2020

Available online 19 August 2020

0169-4332/ © 2020 Elsevier B.V. All rights reserved.

N-doping [21]. The presence of oxygen containing functional groups on the surface of activated carbons and high microporosity were reported as important parameters in the enhancement of the gravimetric H₂ storage capacity of the adsorbents (total uptake of 8.1 wt% at 77 K and 20 bar pressure) [2].

In this study, we experimentally explored the relationship between the oxygen and nitrogen-containing groups on a series of activated carbons with their CH₄ and H₂ adsorption capacity. The structural properties of the final adsorbents were characterised using elemental analysis, Boehm titration, and surface area analysis. The density functional theory (DFT) calculations were performed to study the gas adsorption capacity of the functionalised AC samples using two well-known approaches of (1) adsorption energy and (2) density of state plots. Moreover, the gas (CH₄ and H₂) adsorption performance of the functionalised ACs were investigated and compared to the current benchmark porous materials. GCMC simulations were conducted to investigate the effects of amine and hydroxyl surface groups on the adsorption of CH₄ and H₂.

2. Materials and methods

2.1. Experimental adsorption

2.1.1. Materials

The high-grade anthracite was collected from Mazino mine in the South Khorasan Province, Iran. High purity chemical substances such as sodium bicarbonate (99.70%), sodium carbonate (99.90%), sodium hydroxide (99.00%), potassium hydroxides (99.99%), hydrochloric acid (37.00%), and nitric acid (65.00%) were purchased from Merck KGA (Germany). Urea with stated purity of 99.00% was provided from Khorasan Petrochemical Company, Iran. Methane and hydrogen with the purity of 99.99% were obtained from Technical Gas Services, UAE. To measure the free space during the adsorption process, helium with ultra-high purity of 99.999% was provided from Sepehr Gas Company, Iran. Nitrogen with stated purity of 99.9%, was supplied by Malaekheh company, Iran.

2.1.2. Preparation of the carbon adsorbents

The activated carbons (ACs) were prepared by chemical activation of anthracite as the raw material. The chemical activation process was carried out according to the optimised activation conditions reported in our previous study [22] to maximise the CH₄ storage capacity of the prepared adsorbents. The specific optimisation condition including chemical impregnation ratio, activation temperature and retention time were obtained via two different well-known methods of surface response methodology and genetic algorithm to be 3 g KOH/g anthracite, 1003 K and 60 min, respectively. Also, the whole activation process was described in the [Supplementary Information](#).

The prepared ACs were oxidised using nitric acid to increase the concentration of their surface oxygen groups [23]. In the acidification step, 4 g of AC was added into 100 ml of 5 mol/L nitric acid and stirred at 353 K for 3 h. The oxidation setup includes a 500 ml round bottom flask, a hot plate with magnetic stirring, a thermometer and an oil bath with proper ability to heat up and control the temperature. Subsequently, the oxidised AC was filtered and rinsed with deionised water to a neutral pH and dried at 393 K, overnight. The oxidised activated carbon is called AC-OX.

Nitrogen-containing groups were introduced to the surface of the prepared ACs by urea-functionalising the samples using a solution of urea and ethanol. The suspensions were subjected to sonication for 45 min in an ultrasound bath at 323 K to improve the solubility of urea in ethanol, before adding the adsorbent powder. The following three final products were termed according to the type of raw samples, and the amount of urea per mass of the used solid:

(i) AC-U: 4 g of AC was added to a homogeneous solution of 10 g of

urea in 40 ml of ethanol.

(ii) AC-OX-U1: 4 g of AC-OX was added to a homogeneous solution of 10 g of urea in 40 ml of ethanol.

(iii) AC-OX-U2: 4 g of AC-OX was added to a homogeneous solution of 15 g of urea in 40 ml of ethanol.

All reactions were completed in the pre-described setup for 12 h at 353 K. Then, the rotary evaporator was utilised for efficient and gentle removal of solvents (ethanol) from the samples by evaporation. Urea-functionalised ACs were dried in the oven at 393 K for 2 h. The calcination process was carried out by heating the urea-impregnated ACs in a tubular furnace from room temperatures to 573 K under the ultra-pure nitrogen flow rate of 650 ml/min for an hour. At the end, the AC samples were purified using excess boiling water to remove any water-soluble decomposition material and dried at 393 K, overnight.

2.1.3. Characterisation of the activated carbons

Elemental analysis of the AC samples was performed by Thermo Finnigan EA 1112 analyser (Thermo Fisher, USA). The packing density of the ACs was measured according to the standard test method of D2854 [24], summarised in the [Supplementary Information](#). The micropore structure of the AC samples was characterised by N₂ adsorption/desorption measurements at 77 K using an automatic adsorption system of Belsorp Mini II (BEL, Japan). The Brunauer Emmett Teller (BET) method was used to determine the surface area of the samples in the relative pressure range of $0.05 \leq P/P_0 \leq 0.3$. The total pore volume of the samples (V_{tot}) was calculated at $P/P_0 = 0.99$ and micropore volumes (V_{mic}) were established based on the non-local density functional theory (NLDFT) model from the adsorption data points up to $P/P_0 = 0.1$ (characterising the pores $< 20 \text{ \AA}$).

The presence of functional groups on all the prepared samples were specified through Fourier Transform Infrared Spectroscopy (FTIR) measurement by KBr pellet method using Thermo Nicolet Avatar-370 spectrometer (Nexus, USA). The infrared region in FTIR spectroscopy was selected in the range of 500 cm^{-1} to 4000 cm^{-1} wave numbers.

A custom-built volumetric adsorption measurement apparatus was used for the analysis of CH₄ and H₂ uptake on the prepared adsorbents at 298 K and pressure up to 40 bar. We have described the details of this sorption measurement system, calibration method and measurement procedure in our previous studies [22,25] and briefly in the [Supplementary Information](#).

2.2. Simulation model and method

2.2.1. DFT calculations

The geometry of the studied system is built of coronene-shaped graphitic basis units, where each unit includes 24 carbon atoms. The plate was fully optimised using an unrestricted hybrid B3LYP functional, consists of Becke's three-parameter hybrid exchange functional (B3) and the correlation functional of Lee, Yang, and Parr (LYP) in conjunction with 6-31G(d) basis set. This level of theory was successfully applied to describe the structural and electronic properties of a hexagonal flake of microporous activated carbon.

Three different functional groups of hydroxyl (OH-), amine (NH₂-) and amide (C(O)NH-) were considered influencing the gas adsorption capacity of the ACs. The graphitic sheet and the functionalised adsorbents were separately optimised using B3LYP/6-31G (d). CH₄ and H₂ can approach the functionalised carbon sheets directly above the centre of the benzene rings. In the initial configuration, the carbon atom of CH₄ molecule or H₂ molecule were separately located at a distance of 4 Å and 2 Å, respectively, far from the centre of the benzene plane as illustrated in [Fig. 1](#). Natural bond orbital (NBO) analysis was performed to calculate the partial atomic charge at the same level of theory. The Gaussian 09 package was used for all the calculations in this study [26]. Furthermore, to understand the interaction of gas molecules (i.e. CH₄ and H₂) and the surface of the edge-functionalised carbons, adsorption

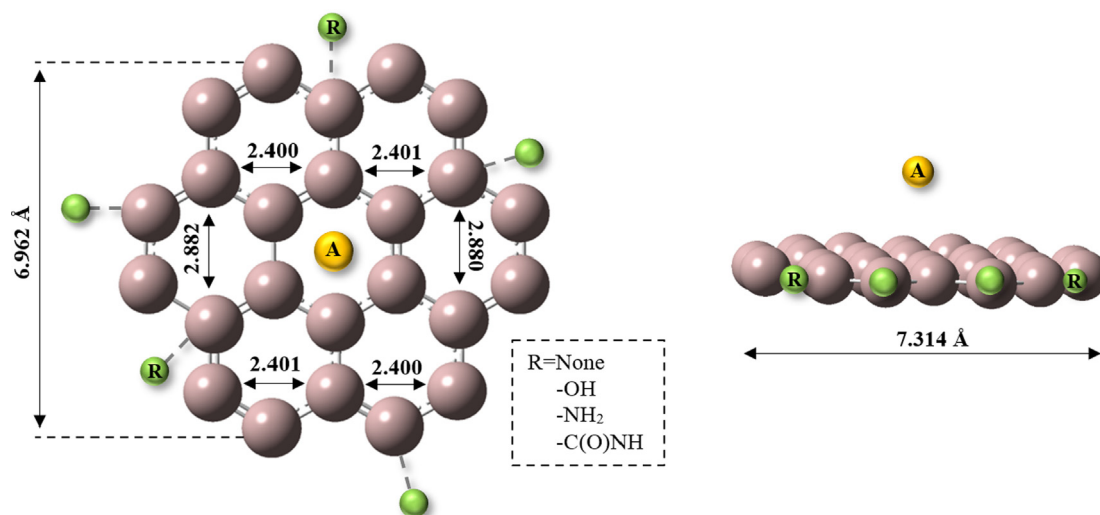


Fig. 1. Initial configurations of gas (CH_4 , H_2) adsorption on edge-functionalised carbon basis unit. The top view (left) and side view (right) are illustrated. Nomenclature: A, adsorbate position above the centre of a benzene ring in basis unit; R, attached functional group. Colour Code: Gray Pink -Carbon, Green -R, Yellow -A.

energy (ΔE_{ads}) is estimated using Eq. (1):

$$\Delta E_{ads} = E_{adsorbate/surf} - (E_{adsorbate} + E_{surf}) \quad (1)$$

where $E_{adsorbate/surf}$ is the total energy of the gas molecule adsorbed on the edge-functionalised carbon's surface, $E_{adsorbate}$ is the energy of the gas species, E_{surf} is the energy of the edge-functionalised carbon's surface.

Introducing functional groups affects the electronic properties of the adsorbents. Herein, we applied the density of state (DOS) analysis to acquire electronic properties of the carbon materials using GaussSum 3 software at the same level of theory (i.e. B3LYP/6-31G (d)).

2.2.2. GCMC simulations

As a powerful and useful tool for investigation on adsorption of gasses, Grand canonical Monte Carlo (GCMC) molecular simulation was used to predict the adsorption isotherms of CH_4 and H_2 on the carbon materials. In the Grand Canonical ensemble in this work, the chemical potential, volume, and temperature are kept constant, while, molecules could be inserted, rotated, displaced and removed in the simulation box to obtain an optimal configuration with the lowest energy of the system [27]. The adsorption isotherms of CH_4 on the ACs were studied at 298 K and pressures of 10, 20, 30 and 40 bar. Furthermore, the adsorption isotherms of H_2 were calculated at 10 and 20 bar, at the same temperature. Equilibrium steps were performed with our optimised grand canonical based molecular simulation codes. Then 10^6 Monte Carlo steps were used to predict adsorption capacities to improve the accuracy of the simulations and reduce the number of iterations [28,29]. The chemical potential at the defined thermodynamic states can be computed from the Peng-Robinson equation of state [32,33].

Intermolecular interaction energy (E) is calculated using the following equation. The electrostatic interaction between two particles is determined via the Coulomb function, and the potential energy of interaction is described by the Lennard-Jones (LJ) function.

$$E_{ij} = 4\epsilon_{ij} \left[\left(\frac{\sigma_{ij}}{r_{ij}} \right)^{12} - \left(\frac{\sigma_{ij}}{r_{ij}} \right)^6 \right] + \frac{q_i q_j}{4\pi D_0 r_{ij}} \quad (2)$$

where r_{ij} is the interatomic distance between the i^{th} and j^{th} atoms or molecules, D_0 is the permittivity of free space ($8.8543 \times 10^{-12} \text{ C}^2/\text{J.m}$), $\left(\sigma_{ij} = \frac{\sigma_i + \sigma_j}{2} \right)$ and $(\epsilon_{ij} = \sqrt{\epsilon_i \epsilon_j})$ are the LJ potential parameters computed by standard Lorentz-Berthelot mixing rules [27].

The interaction energy between a fluid molecule and activated carbon atoms is represented by Steele's 10-4-3 potential [30]:

$$\Phi_{sf} = 2\pi\rho_s \epsilon_{sf} \sigma_{sf}^2 \Delta \left[0.4 \left(\frac{\sigma_{sf}}{z} \right)^{10} - \left(\frac{\sigma_{sf}}{z} \right)^4 - \left(\frac{\sigma_{sf}^4}{3\Delta(0.61\Delta + z)^3} \right) \right] \quad (3)$$

where ρ_s is solid density, Δ is the distance between the lattice planes of the carbon activated, z is the distance between a gas molecule and one of the carbon activated surfaces, σ_{sf} and ϵ_{sf} are obtained by Lorentz-Berthelot mixing rules, similarly.

2.2.3. Molecular model

A slit pore model was used for activated carbon to simplify the GCMC simulation [31]. In the recent studies on molecular simulations of activated carbon, single-layer and three-layer graphite sheets models have been widely used [31]. In this work, a three-layer graphite sheet model was applied. The simulation box length in the case of slit pore is at least 10 times of the collision diameter, which is 3.4 Å for a carbon atom in the graphite layer [32]. Thus, the dimensions of the sheets were considered to be (36×36) Å and periodic boundary conditions are applied in x and y directions. The pore size of graphite lattice was considered 10 Å and the cut-off radius was set to be 18 Å. To study the effect of functional groups on adsorption properties of the solids, the hydroxyl ($\text{OH}-$) and amine (NH_2-) groups were positioned at the corners of slit pore walls.

Fig. 2 shows a schematic diagram of a three-layer graphite pore model of activated carbon with different functional groups. The applied forcefield parameters to represent graphite surfaces are based on the work of Do et al. [32]. Also, the amine and hydroxyl functional groups were described by classical OPLS forcefield parameters [33].

Mostly CH_4 is modelled as a spherical particle with one interaction site, the 1-site model is suitable for describing the adsorption properties, and it is cheaper in terms of computation time. However, to better demonstrate the influence of functional groups in the adsorbent lattice and obtain accurate results, the 5-site Kollman model was selected in the simulation; one site was placed at the centre of the carbon atom, and the other four sites were placed at the centre of four hydrogen atoms [34]. The coordinates of the carbon site and hydrogen sites are given in Table 1.

H_2 was modelled as a spherical rigid molecule, and the forcefield is taken from Cheng et al. [35]. For the H_2 molecule, quantum effects on the adsorption must be considered when H_2 molecules are under confinement. So the Feynman-Hibbs equation (Eq. (4)) was employed for molecular interactions to consider the quantum nature of H_2 [36].

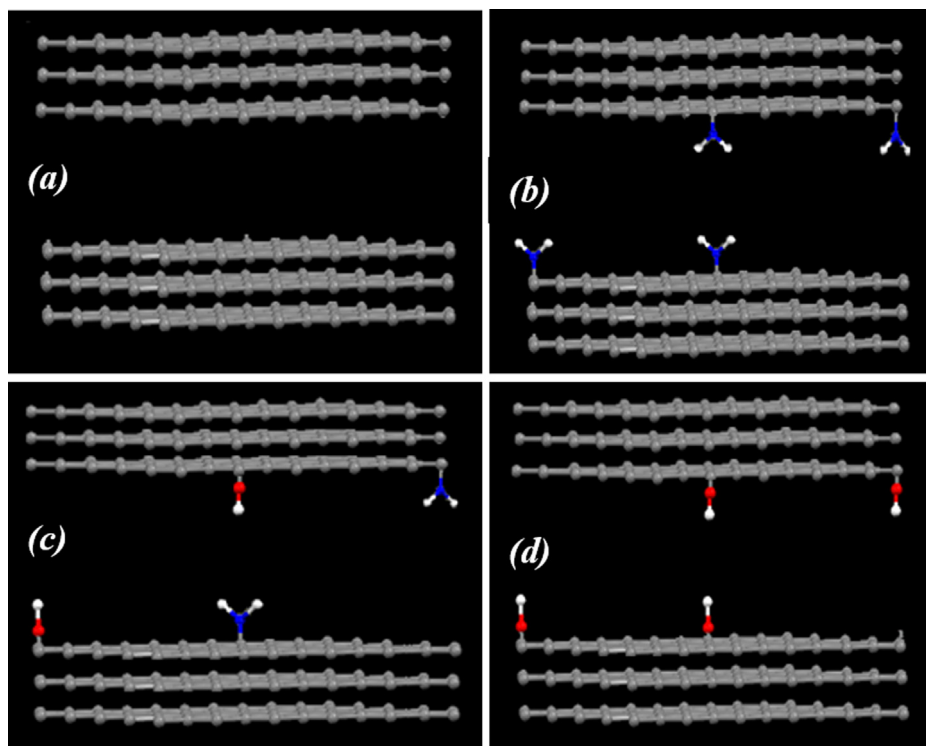


Fig. 2. Activated carbon model of (a) three-layer graphite, (b) graphite wall with amine groups, (c) graphite wall with hydroxyl groups, and (d) graphite wall with amine and hydroxyl groups.

Table 1
Molecular Coordinates of the Five-Sites methane model.

Site	X	Y	Z
Carbon	0	0	0
Hydrogen 1	0	$d\sqrt{3}/3^*$	$-a/3^{**}$
Hydrogen 2	$-d/2$	$-d\sqrt{3}/6$	$-a/3$
Hydrogen 3	$d/2$	$-d\sqrt{3}/6$	$-a/3$
Hydrogen 4	0	0	a

*d is the distance joining two sites and is obtained by $d^2 = 2a^2(1 - \cos\theta)$ and θ is 109.5° . **a is the carbon-hydrogen bond length which is considered 1.09 \AA [33].

$$E_{ij} = 4\epsilon_{ij} \left[\left(\frac{\sigma_{ij}}{r_{ij}} \right)^{12} - \left(\frac{\sigma_{ij}}{r_{ij}} \right)^6 + \frac{h^2}{24m_r K_B T} \left(\frac{132}{r_{ij}^2} \right) \left(\frac{\sigma_{ij}}{r_{ij}} \right)^{12} - \left(\frac{30}{r_{ij}^2} \right) \left(\frac{\sigma_{ij}}{r_{ij}} \right)^6 \right] \quad (4)$$

where $(m_r^{-1} = m_i^{-1} + m_j^{-1})$ is the reduced mass of a pair of interacting molecules, K_B and h are Boltzmann and Planck constants, respectively [35].

The *LJ* parameters for both CH_4 and H_2 interacting with carbon atoms of graphite and other functional groups were adjusted to match the experimental data. The forcefield parameters of adsorbate molecules and adsorbent lattice are presented in Table 2.

3. Result and discussion

This section can be divided into two distinctive parts: (i) experimental results where CH_4 and H_2 adsorption capacity of the ACs were reported and meticulously discussed, (ii) evaluating the GCMC simulation output for predicting gas storage properties of the treated and untreated ACs.

Table 2
Lennard Jones parameters and atomic partial charges for adsorbates, adsorbent and functional groups.

Molecule	atom	q	ϵ/k_B (K)	σ (Å)	Ref.
Hydrogen	H	0	36.70	2.95	[35]
	C	-0.66	55.055	3.4	[32]
Methane	H	0.165	7.901	2.64	
	C	0.18	35.22	3.55	[33]
	N	-0.9	85.54	3.3	
Amine group	H	0.36	0	0	
	C	0.265	52.838	3.75	[33]
	O	-0.7	85.54	3.07	
Hydroxyl group	H	0.435	0	0	
	C	0	28	3.4	[32]

Table 3
Proximate analysis of raw anthracite as the precursor and ultimate analysis of all the anthracite-based samples.

Sample	Proximate analysis (%)				Oxygen ^a
	Carbon	Ash	Volatile matter	Moisture	
Raw Anthracite	86	8.10	5.40	0.50	
Sample	Ultimate analysis (%)				
	Carbon	Hydrogen	Nitrogen	Sulfur	Oxygen ^a
Raw Anthracite	86.10	1.90	0.79	1.70	9.51
AC	83.30	2.01	0.68	0.70	13.31
AC-U	83.91	1.87	0.77	0.97	12.48
AC-OX	61.64	1.70	1.01	0	35.65
AC-OX-U1	68.51	1.53	4.02	0	25.94
AC-OX-U2	66.92	1.66	5.37	0	26.05

^a Calculated by difference.

3.1. Experimental results

3.1.1. Characterisation of the prepared carbon materials

Table 3 shows the elemental analysis of the AC samples. The results

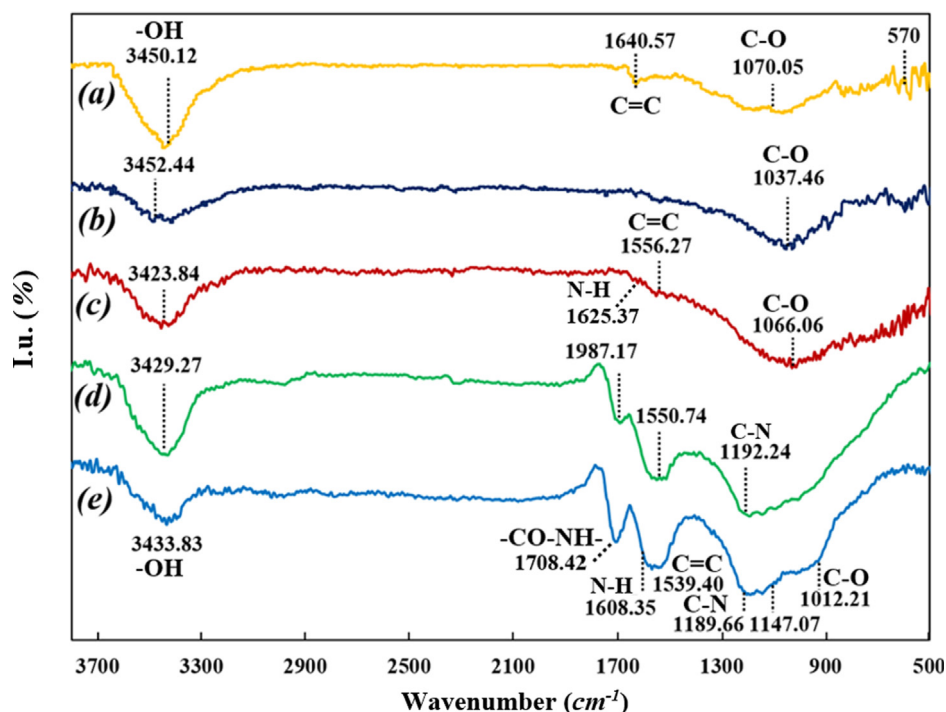


Fig. 3. FT-IR spectra of (a) raw anthracite, b) AC, c) AC-U, d) AC-OX and e) AC-OX-U.

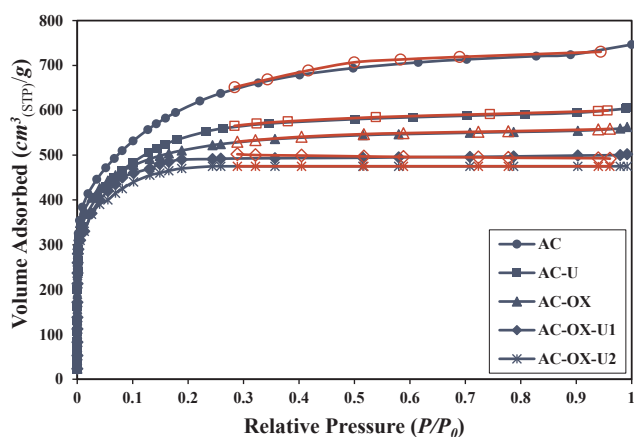


Fig. 4. N_2 adsorption/desorption isotherms for activated coal-based samples of: ●, AC; ■, AC-U; ▲, AC-OX; ◆, AC-OX-U1; *, AC-OX-U2. Filled and empty symbols represent the nitrogen adsorption and desorption, respectively.

obtained from CHN analysis proves an increase in the nitrogen contents after urea treatment, particularly for the pre-oxidised samples. With nitrogen content of 5.37%, the incorporation of nitrogen on AC-OX-U2 (with pre-oxidation) is significantly higher than the loading on the AC sample without oxidation (AC-U, the nitrogen content of 0.77%). The main reason for the nitric acid treatment as an intermediate stage was to enhance the oxygenated anchoring sites on the surface of the porous carbon materials before the modification with nitrogen-containing groups [37,38]. In the urea treatment, these oxygen surface groups play a crucial role as a linking agent for grafting nitrogen-containing functional groups [38]. Therefore, The substantial difference in nitrogen contents between AC-OX-U2 and AC-U denotes the presence of functional oxygen groups on the AC's surface before urea nitridation [37].

The FTIR spectrums of the coal-based carbon samples, which are demonstrated in Fig. 3, were used to investigate the impact of oxidation and amination treatment on the AC's surface functional groups. The peaks around $1000\text{--}1200\text{ cm}^{-1}$ can be assigned to the C-O or C-N

stretching vibration [15]. Moreover, the characteristic adsorptions in the region of $1500\text{--}1600\text{ cm}^{-1}$ specifies the presence of an aromatic C = C ring stretching in the carbon structure of the ACs [38].

For the un-treated activated carbon (spectrum (b)), a peak around 1037 cm^{-1} region can be attributed to the C-O stretching of ethers or ester groups [38]. After the acid treatment (AC-OX), the characteristic adsorption assigned to C = O stretching in carboxylic groups appears at about the wavenumber region of 1550 cm^{-1} .

Urea treatment makes some changes in the spectra of the AC-U and AC-OX-U: a peak around 1600 cm^{-1} can be related to the vibration of N-H from the primary amino groups ($\text{NH}_2\text{-}$) for both of the samples [39]. Also, for the spectrum (e), the presence of a peak at 1708 cm^{-1} may indicate the formation of amide (-CO-NH-) groups during the contact of oxidised activated carbon with urea solution. Furthermore, the broadband in the region of $3420\text{--}3452\text{ cm}^{-1}$ is assigned with overlapping bands of O-H and N-H stretching vibrations, which might be related to the formation of hydrogen bonds between the adsorbed NH_3 molecules and oxygen surface groups [2]. The current observations by the FTIR analysis indicated that the desired functional groups (such as N-H and C-N) were successfully incorporated into ACs structure.

N_2 adsorption/desorption isotherms at 77 K for all five coal-based samples are illustrated in Fig. 4, and their calculated surface area and pore characteristics are summarized in Table 4. All the samples share

Table 4
Nitrogen contents, textural properties and packing density of the prepared AC samples.

Sample	N_2 (%)	S_{BET} (m^2/g)	V_{tot} (cm^3/g)	V_{mic} (cm^3/g)	d_{ave} (Å)	V_{mic}/V_{tot}	ρ^s (g/cm^3)
AC	0.68	2163	1.06	0.74	18.5	0.69	0.54 ± 0.03
AC-U	0.77	1924	0.92	0.62	18.9	0.68	0.57 ± 0.03
AC-OX	1.01	1878	1.14	0.59	19.1	0.51	0.58 ± 0.03
AC-OX-U1	4.02	1695	0.88	0.56	20.7	0.64	0.60 ± 0.03
AC-OX-U2	5.37	1617	0.85	0.53	21.0	0.62	0.60 ± 0.03

* Packing density or bulk density calculated by pressing the powder to $500\text{ kg}/\text{cm}^2$.

almost similar isotherm shape of Type I (microporous solids), where the N_2 uptake rapidly happened at low relative pressures and gradually occurred at medium P/P_0 range. However, the adsorption isotherm of AC (with no modification) is a combination of Type I and Type IV, indicating a slight hysteresis loop at the central region of P/P_0 [40]. These results imply the presence of an abundant number of micropores along with the adequate amount of mesopores in the solid structure of the ACs sample [41,42]. In general speaking, functionalisation has a reducing impact on the BET surface area of the treated samples in the order of AC-U > AC-OX > AC-OX-U1 > AC-OX-U2.

As it is clear from Table 4, nitric acid oxidation leads to enlargement of the total pore volume and decreases the micropore volume and BET surface area of the AC sample. Since nitric acid considered as a strong oxidising agent, oxidation-rich groups will be introduced to the surface of the carbon materials. This functionality has profound effects on the matrix structure of the ACs, including (i) erosion and pore-widening, (ii) blocking the pore entrance [13].

A comparison between AC-U and AC-OX-U series shows the pre-oxidation of the AC sample before the amination step leads to a higher decrease in the surface area, total pore volume, and micropore volume of the corresponded AC samples. The higher density of the introduced nitrogen-containing groups to the AC-OX-U series causes the development of steric hindrances and probably prevention of N_2 diffusion into the micropores [43].

Fig. 5 presents the pore size distribution (PSD) for five AC samples. All the ACs share an almost similar trend of pores distribution: mainly in the micropore range and only a small proportion is larger than 20 Å. The PSD curves for the AC and AC-U samples follow a bi-modal trend; for the AC at around 10.57 Å (sharp peak) and 18.96 Å (modest peak); for the AC-U at about 9.8 Å (sharp peak) and 19.95 Å (weak peak) [15,37]. The three modified adsorbents of AC-OX, AC-OX-U1, and AC-OX-U2 possess a dominant pore size in the range of 9–11 Å, which is desirable for CH_4 adsorption [41,44,45]. On the other hand, the pore diameter in the range of 5–20 Å is reported to be favourable for H_2 uptake [46,47]. Accordingly, all the prepared samples are capable of storing H_2 . Further explanations about the impact of PSD on the gas storage properties of the activated carbons will receive attention later in the gas adsorption section.

The Boehm titration analysis was recruited to study the surface chemistry of the representative samples. A schematic of the Boehm technique depicted in Fig. 6. Details of the method was reported before [48,49] and briefly in the Supplementary Information. The results of the acid-basic properties of all the samples are listed in Table 5.

From Table 5, it is evident that the chemical treatments have a significant impact on acid-base surface values of the carbon materials. While the extent of basic groups on AC decreases nearly to zero after the oxidation with HNO_3 , the number of acidic groups increases

considerably (about 5 times higher than the raw AC). On the other hand, during the urea treatment, the surface nitrogen-containing groups sharply increase the value of total basicity, especially for the pre-oxidised samples (AC-OX-Us) [38,43].

3.1.2. Methane adsorption

Fig. 7 shows the gravimetric and volumetric CH_4 adsorption isotherms for all five AC samples at 298 K and pressures up to 40 bar. Also, the experimental data for the CH_4 adsorption at different temperatures $T = (298, 310, \text{ and } 320) \text{ K}$ are reported in the Supplementary Information (see Table S1 and Fig. S2). The adsorption isotherms resemble Type I (IUPAC isotherm, which is individual for the microporous materials [15]. AC-OX shows the lowest amount of CH_4 stored in both gravimetric (9.41 mmol/g) and volumetric ($125 \text{ cm}^3_{(STP)}/\text{cm}^3$) basis. Although AC-OX has a higher surface area of $1878 \text{ m}^2/\text{g}$ and micropore volume ($0.59 \text{ cm}^3/\text{g}$) in comparison with the AC-OX-Us, AC-OX shows the lowest CH_4 uptake. These results suggest that the strong electronegative O atom in the functional groups repels the electronegative C atom in the CH_4 molecule, which possibly results in declining the CH_4 adsorption capacity of the sample [17]. Introducing the nitrogen-containing groups to the surface of ACs has a positive effect on the adsorption of CH_4 and promotes the storage capacity in the sequence of AC-OX-U1 > AC-OX-U2 > AC-U over the high-pressure range.

Closer inspection in Fig. 7(a) reveals that the adsorption isotherms could be divided into three sections; where zone I, II and III happen in the pressure ranges of 0–10 bar, 10–20 bar and 20–40 bar respectively. At zone (I), the amount of CH_4 uptake is almost equal in both samples of AC and AC-U and exceeded the capacity of the other adsorbents. The microporosity of AC and AC-U is one of the reasons for the relatively high storage capacity of these adsorbents (see Table 4) [50,51]. A linear relationship between the CH_4 uptake capacity and porosity characteristics of microporous carbons was reported in the literature [44,52]. Our previous studies showed adsorbents with well-developed micropores and narrow mesopores, similar to the AC and AC-U samples in this study, are favourable for CH_4 storage application [22,25].

In zone (II), pressures between 10 and 20 bar, the CH_4 storage capacity of the AC-OX-U series rises and becomes close to the CH_4 uptake values for AC-U (10.89 mmol/g) and AC (10 mmol/g) samples. Based on these results, it can be concluded that the amount of adsorbed CH_4 in the second region, relies on the competition between two fundamental properties of appropriate pore size distribution and the surface chemistry [15,17,18]. It needs to be noted that the CH_4 adsorbed quantity of 10.95 mmol/g for AC-OX-U1 is among the highest storage capacities reported for microporous carbon matters at similar experimental conditions [1,15,41,42].

In the last section of the adsorption isotherm (zone III), despite a high surface area and well-developed microporosity of AC, the modified adsorbents show comparatively higher CH_4 uptake in the order of AC-OX-U1 (14.2 mmol/g), AC-U (14 mmol/g) and AC-OX-U2 (13.8 mmol/g). The reason for such an enhancement is possibly due to the positive effect of nitrogen-containing functional groups on the surface of these samples. In comparison with all the prepared samples, the pre-oxidised + aminated carbons display enhancement in CH_4 adsorption at room temperatures. These results were obtained at the condition that the pristine AC and AC-U possess the highest micropore volume (0.74 and $0.62 \text{ cm}^3/\text{g}$, respectively) among all the samples. Accordingly, it seems the changes in the surface chemistry of the ACs can dominantly affect their CH_4 uptake capacity, particularly when the carbon surface is saturated with basic oxygen and nitrogen functional groups [37,38]. The CH_4 storage capacities of the AC-OX-Us and AC-U, which are originated from inexpensive precursors and prepared via a cost-effective procedure, are comparable or even exceeded those reported in the literature: 14.9 mmol/g on Anthracene Al-soc-MOF-3, 8.5 mmol/g for Co (bdp), and 10.2 mmol/g on Fe(bdp) [53,54].

Although the gravimetric adsorption capacity of the adsorbents

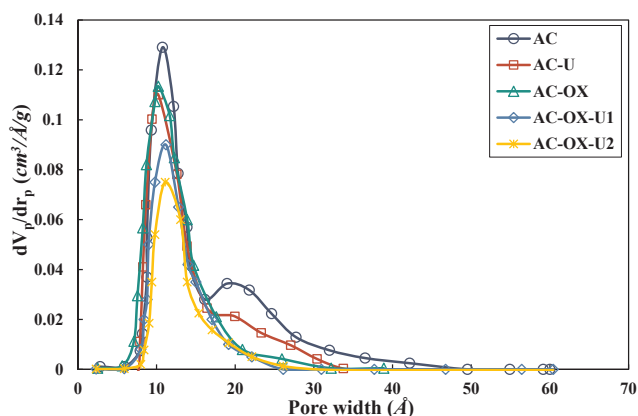


Fig. 5. Pore size distribution for the activated samples of: ○, AC; □, AC-U; △, AC-OX; ◇, AC-OX-U1; *, AC-OX-U2.

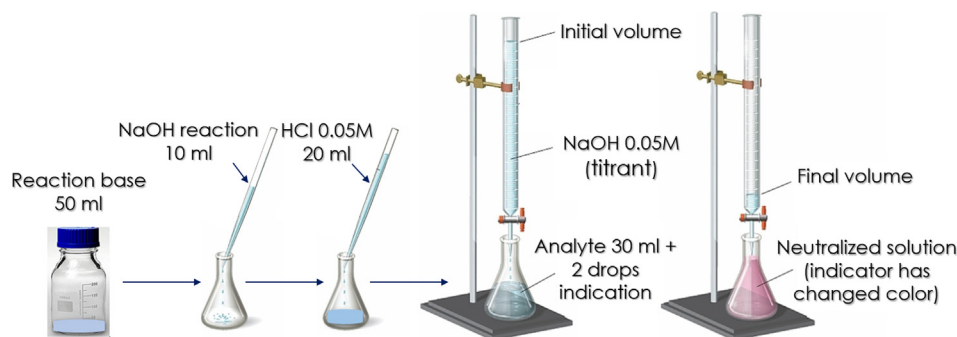


Fig. 6. Schematic of the recommended Boehm technique.

Table 5

Result of Surface groups on the treated and un-treated ACs samples obtained from Boehm titrations.

Sample	Carboxyl (mmol/g)	Lactone (mmol/g)	Phenol (mmol/g)	Total acidity (mmol/g)	Total basicity (mmol/g)
AC	0.0595	0.0427	0.0803	0.1825	0.0675
AC-U	0.0590	0.0419	0.0775	0.1784	0.0685
AC-OX	0.3897	0.1167	0.4167	0.9231	0.0082
AC-OX-U1	0.0548	0.0643	0.1902	0.3093	0.0781
AC-OX-U2	0.0572	0.0652	0.1884	0.3208	0.0773

depends on their pore texture (microporosity) and surface chemistry characteristics, the volumetric capacity is strongly affected by the packing density of the materials [2,42]. The calculation method of CH₄ volumetric capacity is presented in the [Supplementary Information](#). As it is depicted in Fig. 7(b), the volumetric capacity of AC-OX-U1 at 28 bar (173 cm³_(STP)/cm³) and 40 bar (190 cm³_(STP)/cm³) is higher than the other samples. The volumetric CH₄ storage capacity of these samples is more significant than many reported values for high surface area porous carbons [41,42,55]. When the high packing density of the modified samples, i.e. 0.60 g/cm³ (AC-OX-Us) and 0.57 g/cm³ (AC-U) is accompanied with their significant gravimetric CH₄ uptake capacity, their volumetric CH₄ storage capacity at 40 bar pressure become almost equal or even higher than many well-known adsorbents such as HKUST1 (193 cm³/cm³), MOF-205 (191 cm³/cm³), MOF-177 (181 cm³/cm³), MOF-210 (168 cm³/cm³) and MOF-200 (147 cm³/cm³) [56,57]. The superior CH₄ adsorption capacity of the AC-OX-Us series and also AC-U makes them promising candidates for vehicular onboard applications.

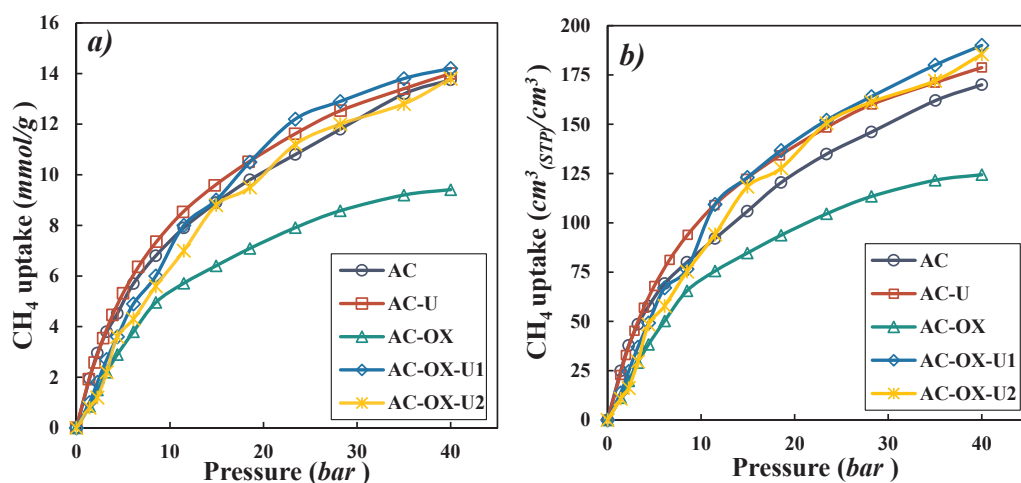


Fig. 7. Methane adsorption isotherms for the activated samples of: ○, AC; □, AC-U; △, AC-OX; ◇, AC-OX-U1; *, AC-OX-U2; at 298 K in a) gravimetric and b) volumetric calculation basis.

3.1.3. Hydrogen adsorption

Fig. 8 shows H₂ adsorption isotherms at 298 K and pressures up to 20 bar in the gravimetric and volumetric basis for all the prepared samples. The adsorption measurement data are also presented in [Table S2](#) of the [Supporting Information](#). At the pressures up to 15 bar, all the adsorption isotherms increase linearly with pressure following Henry's law, implying the H₂ adsorption at ultra-micropores [58]. The AC sample with 0.6 mmol/g (7 cm³_(STP)/cm³) and AC-OX-U1 with 0.26 mmol/g (3.50 cm³_(STP)/cm³) H₂ adsorption at 20 bar show respectively the maximum and minimum amount of H₂ uptake in both gravimetric and volumetric basis. The lowest H₂ capacity of AC-OX-U1 can be interpreted by the steric hindrance effect of urea functional groups on the surface of the corresponded adsorbent, which leads to a diminishing chance for H₂ molecules to entering into the micropores [37,59]. The effect of oxygen-rich surfaces and urea modification on H₂ adsorption is apparent on AC-OX (0.44 mmol/g, 5.71 cm³_(STP)/cm³) and AC-U (0.39 mmol/g and 5 cm³_(STP)/cm³), respectively.

The H₂ adsorption measurement results imply that larger micropore volume is preferable to increase the H₂ storage capacity of carbon-based materials, mainly due to the strong interaction of carbon and hydrogen molecules [2,60] and the inductive effect of surface chemistry has a secondary role in H₂ uptake.

3.2. DFT calculations and GCMC simulation

The effect of functionalisation were investigated for all the modified activated carbons by using a systematic theoretical investigation including adsorption energy, density of state and GCMC simulation.

3.2.1. Adsorption energy

The optimised adsorption configuration of CH₄ and H₂ on the AC, AC-U, AC-OX, and AC-OX-Us samples depicted in [Fig. 9\(a-d\)](#) and

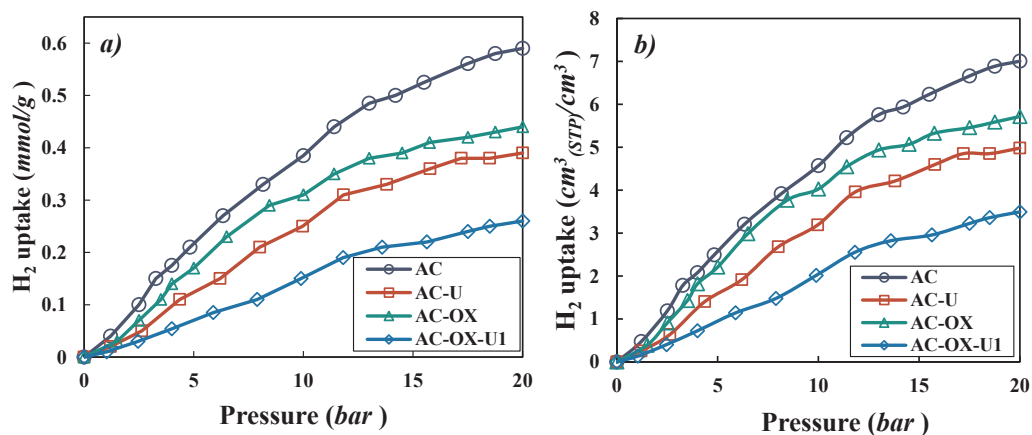


Fig. 8. H₂ adsorption isotherms for the activated samples of: ○, AC; □, AC-U; △, AC-OX; ◇, AC-OX-U1; *, AC-OX-U2; at 298 K in a) gravimetric and b) volumetric calculation basis.

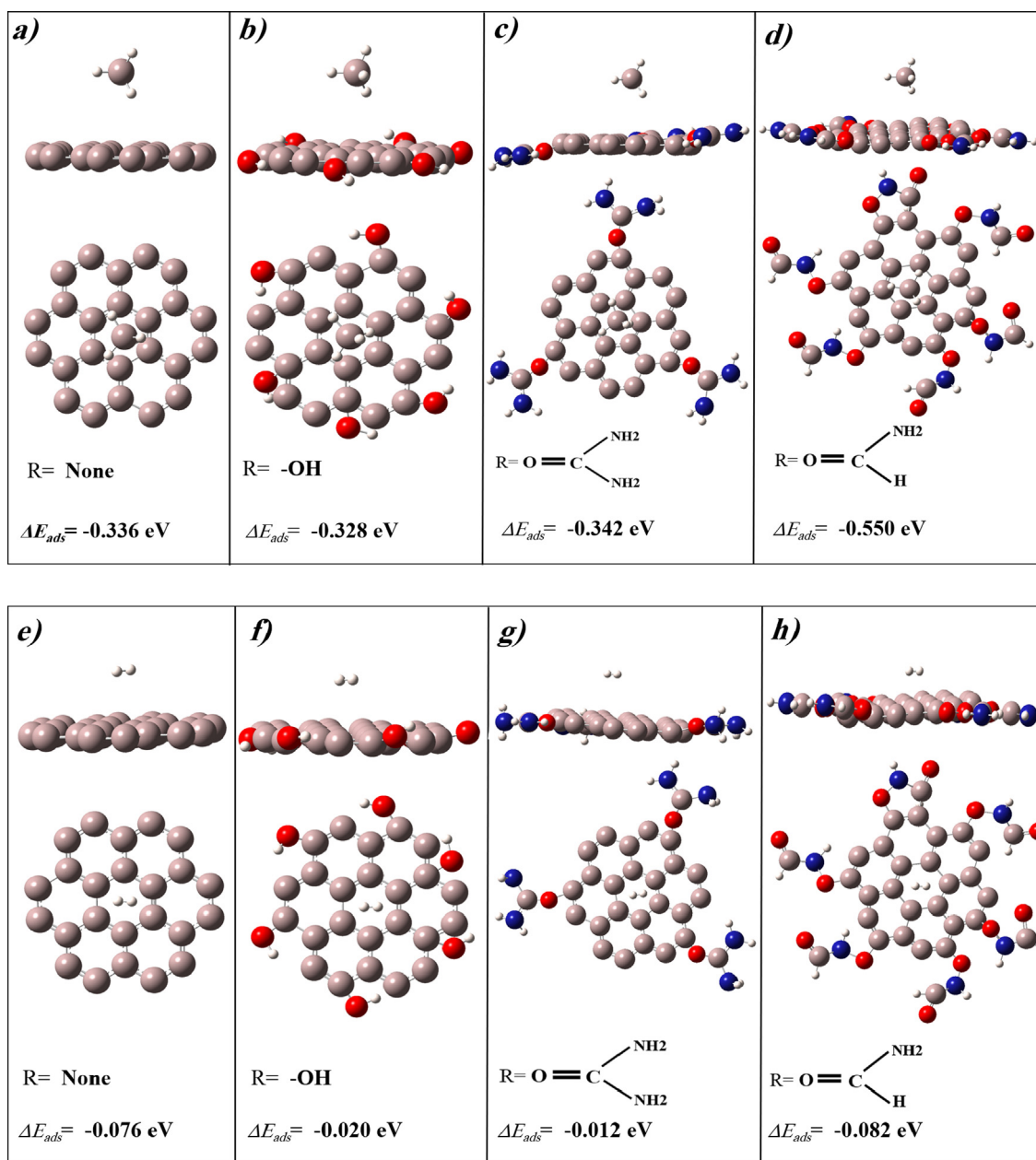


Fig. 9. Stable adsorption configurations (side view (up) and top view (down)) for CH₄ on (a) AC, (b) AC-OX, (c) AC-U and (d) AC-OX-U1 and for the H₂ on (e) AC, (f) AC-OX, (g) AC-U and (h) AC-OX-U1. The visualized colours of gray-pink, white, red and blue, respectively represent the atoms of carbon, hydrogen, oxygen, and nitrogen.

Fig. 9(e-h), respectively. To understand the interaction between the adsorbate and the edge-functionalised microporous carbon surface, the adsorption energies were calculated, and the values are reported in Fig. 9. The negative amounts of adsorption energy show a stable exothermic reaction [61]. The results indicate that the functionalisation has a considerable inductive impact on the gas adsorption properties of the carbon unit surfaces.

In the case of the CH_4 /adsorbent systems, adsorption energy is 0.336 eV for the basic AC unit, which is slightly lower than the 0.342 eV of the AC-U. The OH^- group weakens the adsorption energy of AC-OX to 0.328 eV [17]. Moreover, for a unit saturated with $\text{C}(\text{O})\text{NH}^-$ (AC-OX-U sample), the adsorption energy enhances up to 0.550 eV. When comparing the adsorption energy of the CH_4 /AC-OX-U system with the AC and AC-U systems, the enhancement percentages are 63.69% and 60.81%, respectively. These results confirm that the functionalised surface site of $\text{C}(\text{O})\text{NH}^-$ is energetically favourable for CH_4 adsorption [17,61].

Two strong electronegative atoms of O and especially N increase the electron density of the carbon surface (AC-OX-U sample). These atoms act as electron donors to the adsorbate molecules near the pore space and effectively guide them to store on adsorbent porosity [17,62]. In other words, the electronegative N and O atoms of the functional groups contributing their electrons to the H atoms of CH_4 and promote the methane adsorption on the corresponded adsorbent, as shown in Fig. 10. It is noteworthy that similar results were obtained experimentally; the AC-OX-U carbons showed higher CH_4 storage capacity in comparison to the other samples (Fig. 7).

For the H_2 /adsorbent systems, the adsorption energy is affected by the electrostatic interaction when the H_2 molecule approaches the

surface functional groups (see Fig. 9(e-h)). The adsorption energy of H_2 for the AC is 0.076 eV, which decreases to 0.010 eV for the AC-U. When the unit is saturated with the $\text{C}(\text{O})\text{NH}^-$ groups (AC-OX-U sample), the adsorption energy is estimated to be 0.085 eV. From a theoretical point of view, the embedding of the $\text{C}(\text{O})\text{NH}^-$ groups can slightly increase the H_2 adsorption. Both nitrogen and oxygen-containing groups introduce negative-charge characteristics to the carbon surface. As a result, the non-polar H_2 molecule may become momentarily polarised and get attracted to the modified adsorbent. However, in the experimental measurements, it was determined that the inductive effect of functional groups does not improve the hydrogen adsorption on the adsorbents, and micropore size distribution is the dominant parameter in the storage of H_2 [46].

3.2.2. The density of state (DOS)

Besides the structural characteristics, the electronic properties of the adsorbents play an essential role in the gas adsorption capacity of these porous materials [17,63,64]. Every single adsorbent shows unique electronic characteristics that can be identified by the DOS analysis. The introduction of functional groups such as OH^- or NH_2^- to the surface of microporous carbons alters the electronic density, as is evident via the DOS plots (Fig. 11). The DOS of CH_4 /activated carbon systems is continuously distributed within the range of -12 eV to 12 eV, which is consistent with the distribution range in the literature [61,63]. The DOS plots for the CH_4 and AC-OX (AC-OH), AC-U (AC- NH_2), and AC-OX-U (AC-OH- NH_2) systems emerge significant peaks comparing with the CH_4 /intrinsic AC. Below the Fermi level¹ (in the range of -12 to 0 eV), the electron density (intensity of the peaks) of the CH_4 /AC-U systems and especially CH_4 /AC-OX-U system, is much higher than the other carbons [65]. The electron density near the Fermi levels (around -4 to 0 eV) is higher for the functionalised samples in the order of AC-OX-U > AC-U > AC-OX.

According to Fig. 11(a), the CH_4 /AC-OX-U system exhibits four pronounced peaks below the Fermi level, which represent high interaction between AC-OX-U and CH_4 . In other words, the current results support the high CH_4 capture ability of microporous samples functionalised with OH^- and NH_2^- groups [17,61]. These observations are consistent with the adsorption energy analysis results and in good agreement with the measured CH_4 storage capacity of the AC-OX-U sample presented in the adsorption measurements section. As discussed in the experimental section, the maximum amount of CH_4 uptake was reported for the AC-OX-U, which is modified through pre-oxidation (OH^-) followed by amination (NH_2^-).

A detailed description of the electronic contributions for the H_2 molecules near the AC samples was analysed using the DOS, and the results are depicted in Fig. 11(b). After introducing the functional groups to the solid's surface, the value of the energy gap was slightly changed near the Fermi level. Consistent with the adsorption energy results, the DOS curves show relatively sharp peaks below the Fermi level for the H_2 /AC-OX-U system. The main reason for the enhanced reactivity can be related to the strong attraction of electronic forces between the surface groups (i.e., oxygen and nitrogen) and the hydrogen orbitals [2,18,66]. On the other side, the presence of the minor peaks for the AC-U and AC-OX carbons indicates that the effect of functionalisation on the electronic density of these materials is almost negligible. Although the DOS results are in favour of the promotion of H_2 adsorption on the surface of the AC-OX-U, simulation results are inconsistent with the experimental findings. Under the real experimental condition, it seems that the slight changes in the DOS plots of the functionalised carbons do not promote the adsorption of non-polar hydrogen molecules. It also appears that the structural properties (i.e. BET surface area and microporosity) dominantly affect the H_2

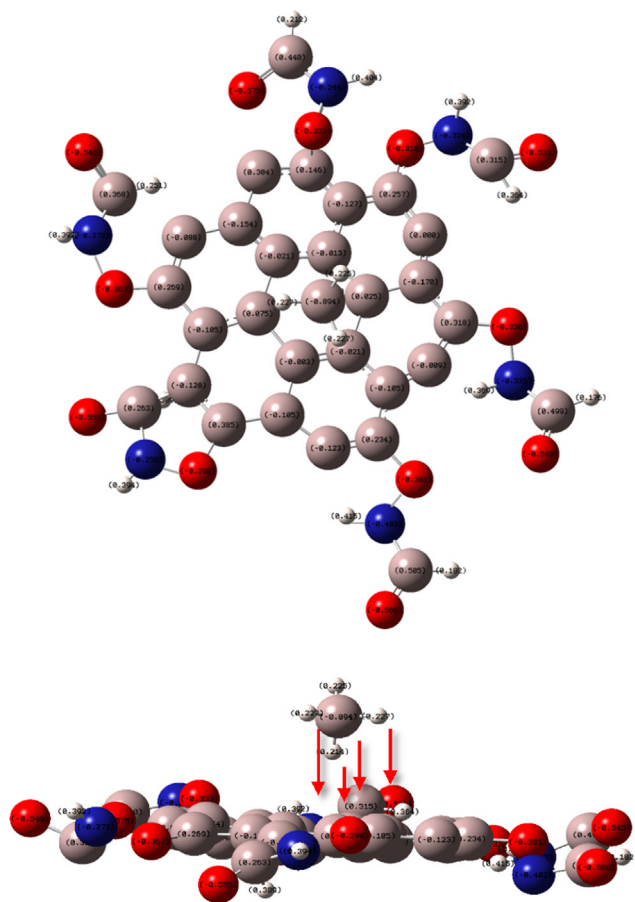


Fig. 10. Schematic display of the interaction between the adsorbate (CH_4) and charged atoms in the functional group of the AC-OX-U adsorbent (top view (up) and side view (down)).

¹ The highest energy level that an electron can occupy at the absolute zero temperature is known as the Fermi Level.

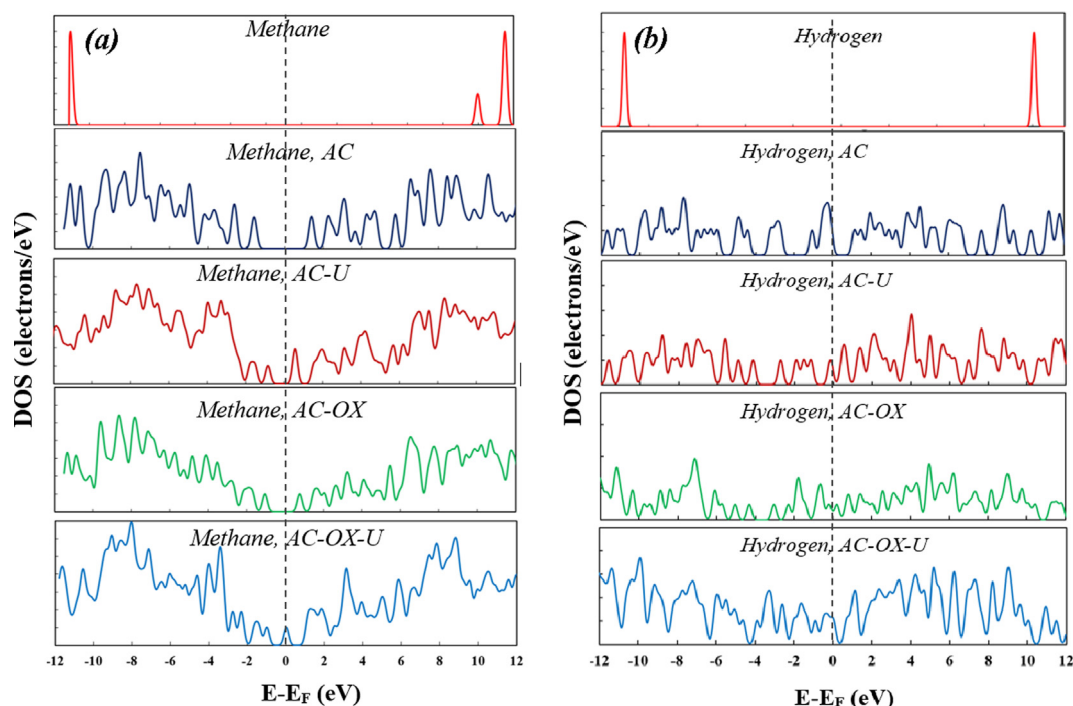


Fig. 11. Density of states (DOS) plots for all carbonaceous adsorbents for adsorption of (a) CH₄ and (b) H₂ molecule. The dotted line represents the Fermi level that is set to zero.

adsorption capacity of the adsorbents [46].

3.2.3. GCMC results

The simulated adsorption isotherms of CH₄ and H₂ on a series of slit pore modelled activated carbons with amine and hydroxyl groups at 298 K are demonstrated in Fig. 12 (a-b), respectively. The results from the GCMC simulations for CH₄ are in an excellent agreement with the measured isotherms over the range of investigated pressures (0–40 bar). The CH₄ adsorption capacity at the defined pressure and temperature decreased in the order of AC-NH₂ (AC-U) > AC > AC-OH-NH₂ (AC-OX-U1) > AC-OH (AC-OX). The addition of functional groups reduces the accessible volume of activated carbons, and as a result, it is expected to reduce their CH₄ adsorption capacity. For AC-OH, the strong electronegative O atoms slightly weaken the CH₄ adsorption, whereas, for the AC-NH₂, corner-functionalisation has a minor positive effect on the CH₄ adsorption capacity, which is different from the negative impact of surface functionalisation on the adsorbed gas amount. In the case of CH₄, a rigid orderly tetrahedron model with five charged Lennard-Jones (*LJ*) interaction describes the adsorbate-adsorbent and the adsorbate-adsorbate interactions properly and the simulation results agree well with the experimental results and the DFT analysis.

As depicted in Fig. 12(b), the simulation results evidently can follow the behaviour of H₂ adsorption on the ACs under real conditions. The GCMC simulation shows that the maximum and the minimum H₂ uptake capacity corresponded to the samples of AC (1.4 mmol/g) and AC-OX-U1 (0.92 mmol/g), respectively. Similarly, the experimental measurements reported maximum and minimum values of H₂ storage for the AC and AC-OX-U1 adsorbents.

However, as it is clear in all the isotherm curves, the simulated H₂ adsorption data are greater than the experimental ones. For instance, at pressure of 10 bar, the simulation result predicts the H₂ adsorption amount of 0.92 mmol/g for the AC sample, while the adsorption measurements report the H₂ storage of 0.39 mmol/g (~57% error). One possible explanation for such a difference can be related to the effect of true solid volume measurement, which was conducted using helium with the assumption of negligible He adsorption. However, He can be adsorbed on the small pores of the samples at ambient temperature and

moderate pressures that affects the measurement of solid's true volume and results in a deviation in gas adsorption measurements [58,67]. The mentioned deviation is more evident in the adsorption of gases with small uptake such as H₂. The other reason for the difference between the measured and calculated H₂ adsorption values is associated with the small molecular size of H₂ and the non-polar modelled H₂ molecules in slit pores. Although the Feynman-Hibbs equation predicts lower adsorbed amount for H₂ than classical Lennard-Jones equation, still adsorption isotherms estimations are relatively high. Unlike CH₄, none of the functional groups help to improve the adsorption of H₂ on the ACs. Since amine groups take more space in the simulation box, the NH₂-group's effect is more significant in reducing the adsorption capacity.

4. Conclusion

A series of nitrogen-doped coal-based activated carbons were synthesized for CH₄ and H₂ storage application. The oxygen- and nitrogen-containing functional groups were introduced to the surface of the prepared activated carbons by oxidation and urea functionalisation of the solids, respectively. The results of ACs characterisation proved that urea and oxidised functional groups were appropriately introduced on the surface of the porous carbons. The functionalisation has a reduction impact on the BET surface area of the treated samples in the order of AC-U > AC-OX > AC-OX-U1 > AC-OX-U2. The samples of AC-OX-U1 with 14.2 mmol/g (190 cm³_{(STP)/cm³}) and AC-OX-U2 with 13.8 mmol/g (180 cm³_{(STP)/cm³}) showed comparatively high CH₄ uptake among the others; the enhancement is likely due to the positive effect of the nitrogen-rich surface of these samples. The density functional theory (DFT) calculations also were performed to study the gas adsorption capacity of the functionalised ACs using two well-known approaches of adsorption energy and the density of state plots. The effects of amine and hydroxyl groups on the adsorption isotherms of the unfunctionalised ACs were investigated by the GCMC method. The theoretical findings provide relatively enhancement in CH₄ adsorption capacity of the modified samples in comparisons with intrinsic AC. Unlike CH₄, it was found that none of the functional groups help to improve the adsorption storage of H₂ on activated carbon.

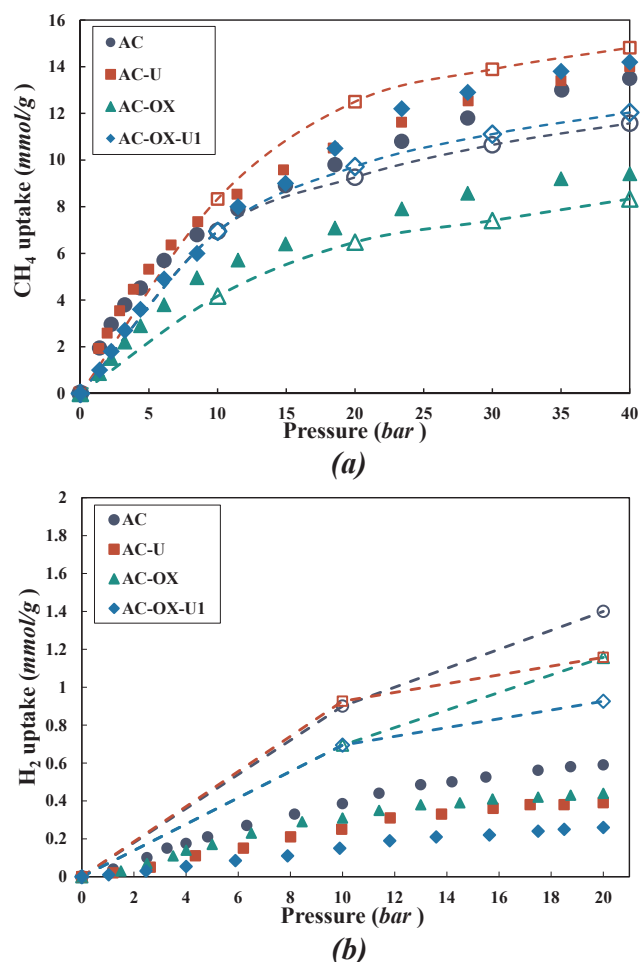


Fig. 12. Computed and measured adsorption isotherms of a) CH_4 and b) H_2 on activated carbons of: ●, AC; ■, AC-U; ▲, AC-OX; ◆, AC-OX-UI; with different functional groups at 298 K. Filled and empty symbols (with dotted lines) represent experiment and GCMC simulation data, respectively.

CRediT authorship contribution statement

Shohreh Mirzaei: Conceptualization, Methodology, Software, Validation, Formal analysis, Investigation, Writing - original draft, Visualization. **Ali Ahmadpour:** Conceptualization, Methodology, Resources, Data curation, Writing - review & editing, Supervision, Project administration, Funding acquisition. **Akbar Shahsavand:** Conceptualization, Software, Formal analysis, Resources, Data curation, Supervision, Project administration, Funding acquisition. **Ali Nakhaei Pour:** Methodology, Software, Validation, Writing - review & editing. **Leila LotfiKatooli:** Conceptualization, Methodology, Software, Validation, Formal analysis, Investigation. **Ali Garmroodi Asil:** Methodology, Software, Formal analysis. **Babak Pouladi:** Conceptualization, Resources, Funding acquisition. **Arash Arami-Niya:** Conceptualization, Methodology, Software, Formal analysis, Writing - review & editing.

Declaration of Competing Interest

The authors declared that there is no conflict of interest.

Acknowledgments

This work is supported by South Pars Gas Complex (Grant Number 306494) and Ferdowsi University of Mashhad, Iran (Grant Number

44340) for Mrs. Mirzaei provided through a Postgraduate Research Scholarship.

The authors express their special thanks to Dr. Babak Pouladi, Dr. Mahboobeh Ghahramani Nejad and Siroos Rostami for their advice and help with the experiments.

Appendix A. Supplementary material

Supplementary data to this article can be found online at <https://doi.org/10.1016/j.apsusc.2020.147487>.

References

- [1] S. Ghosh, R. Sarathi, S. Ramaprabhu, Magnesium oxide modified nitrogen-doped porous carbon composite as an efficient candidate for high pressure carbon dioxide capture and methane storage, *J. Colloid Interface Sci.* 539 (2019) 245–256.
- [2] T.S. Blankenship II, N. Balahmar, R. Mokaya, Oxygen-rich microporous carbons with exceptional hydrogen storage capacity, *Nat. Commun.* 8 (2017) 1545.
- [3] M. Beckner, A. Dailly, Hydrogen and methane storage in adsorbent materials for automotive applications, *Int. J. Energy Res.* 40 (2016) 91–99.
- [4] Q. Xue, M. Wu, X.C. Zeng, Jena P. Correction, Co-mixing hydrogen and methane may double the energy storage capacity (*Journal of Materials Chemistry A* (2018), *J. Mater. Chem. A* 6 (2018).
- [5] A. Ayati, A. Ahmadpour, F.F. Bamoharram, B. Tanhaei, M. Mänttari, M. Sillanpää, A review on catalytic applications of Au/TiO₂ nanoparticles in the removal of water pollutant, *Chemosphere* 107 (2014) 163–174.
- [6] A. Ahmadpour, H. Rashidi, M.J.D. Mahboub, M.R. Farmad, Comparing the performance of KOH with NaOH-activated anthracites in terms of methane storage, *Adsorpt. Sci. Technol.* 31 (2013) 729–745.
- [7] A. Okhovat, A. Ahmadpour, A comparative study of the effects of different chemical agents on the pore-size distributions of macadamia nutshell-based activated carbons using different models, *Adsorpt. Sci. Technol.* 30 (2012) 159–169.
- [8] A. Ahmadpour, D. Do, Characterization of modified activated carbons: equilibria and dynamics studies, *Carbon* 33 (1995) 1393–1398.
- [9] A. Ahmadpour, N. Jahanshahi, S. Rashidi, N. Chenarani, M.J.D. Mahboub, Application of artificial neural networks and adaptive neuro-fuzzy inference systems to predict activated carbon properties for methane storage, *Adsorpt. Sci. Technol.* 32 (2014) 275–290.
- [10] S. Rostami, A. Nakhaei Pour, M. Izadyar, Hydrogen adsorption by g-C₃N₄ and hydrogen oxide nanosheets, *J. Nanostructures.* 9 (2019) 498–509.
- [11] S. Rostami, A. Nakhaei Pour, M. Izadyar, A short review on modified carbon materials: promising materials for hydrogen storage, *Sci. Prog.* 101 (2018).
- [12] X. Chen, J. Zhang, B. Zhang, S. Dong, X. Guo, X. Mu, et al., A novel hierarchical porous nitrogen-doped carbon derived from bamboo shoot for high performance supercapacitor, *Sci. Rep.* 7 (2017) 7362.
- [13] S. Hao, J. Wen, X. Yu, W. Chu, Effect of the surface oxygen groups on methane adsorption on coals, *Appl. Surf. Sci.* 264 (2013) 433–442.
- [14] B. Huang, G. Liu, P. Wang, X. Zhao, H. Xu, Effect of nitric acid modification on characteristics and adsorption properties of lignite, *Processes.* 7 (2019) 167.
- [15] Y. Li, R. Xu, B. Wang, J. Wei, L. Wang, M. Shen, et al., Enhanced N-doped porous carbon derived from KOH-activated waste wool: A promising material for selective adsorption of CO₂/CH₄ and CH₄/N₂, *Nanomaterials* 9 (2019) 266.
- [16] M.S. Shafeeyan, W.M.A.W. Daud, A. Houshmand, A. Arami-Niya, Ammonia modification of activated carbon to enhance carbon dioxide adsorption: Effect of pre-oxidation, *Appl. Surf. Sci.* 257 (2011) 3936–3942.
- [17] X. Lu, D. Jin, S. Wei, M. Zhang, Q. Zhu, X. Shi, et al., Competitive adsorption of a binary CO₂-CH₄ mixture in nanoporous carbons: effects of edge-functionalization, *Nanoscale* 7 (2015) 1002–1012.
- [18] J.S. Im, M.J. Jung, Y.-S. Lee, Effects of fluorination modification on pore size controlled electrospun activated carbon fibers for high capacity methane storage, *J. Colloid Interface Sci.* 339 (2009) 31–35.
- [19] X. Liang, S.-P. Ng, N. Ding, C.-M.L. Wu, Strain-induced switch for hydrogen storage in cobalt-decorated nitrogen-doped graphene, *Appl. Surf. Sci.* 473 (2019) 174–181.
- [20] F. Akbari, A. Reisi-Vanani, M.H. Darvishnejad, DFT study of the electronic and structural properties of single Al and N atoms and Al-N co-doped graphyne toward hydrogen storage, *Appl. Surf. Sci.* 488 (2019) 600–610.
- [21] Y. Xia, G.S. Walker, D.M. Grant, R. Mokaya, Hydrogen storage in high surface area carbons: experimental demonstration of the effects of nitrogen doping, *J. Am. Chem. Soc.* 131 (2009) 16493–16499.
- [22] S. Mirzaei, A. Ahmadpour, A. Shahsavand, H. Rashidi, A. Arami-Niya, A Comparative study between regression and soft computing models to maximize methane storage capacity of anthracite-based adsorbents, *Ind. Eng. Chem. Res.* (2020).
- [23] A. Arami-Niya, T.E. Rufford, Z. Zhu, Activated carbon monoliths with hierarchical pore structure from tar pitch and coal powder for the adsorption of CO₂, CH₄ and N₂, *Carbon* 103 (2016) 115–124.
- [24] D2854-09(2014) A. Standard Test Method for Apparent Density of Activated Carbon. ASTM International, West Conshohocken, PA; 2014. p. www.astm.org.
- [25] Mirzaei SA, A.; Shahsavand, A.; Rashidi, H.; Arami-Niya, A. Superior performance of modified pitch-based adsorbents for cyclic methane storage. *Journal of Energy Storage.* 2020.
- [26] Gaussian09 RA. 1, mj frisch, gw trucks, hb schlegel, gc scuseria, ma robb, jr

- cheeseman, g. Scalmani, v. Barone, b. Mennucci, ga petersson et al., gaussian. Inc, Wallingford CT. 2009;121:150-66.
- [27] D. Frenkel, B. Smit, Understanding molecular simulation: from algorithms to applications, Elsevier (2001).
- [28] L. Loftikatooli, A. Shahsavand, Reliable prediction of adsorption isotherms via genetic algorithm molecular simulation, *J. Mol. Model.* 23 (2017) 33.
- [29] L. Loftikatooli, A. Shahsavand, An innovative approach for molecular simulation of nanostructured adsorption isotherms via the ant colony method, *J. Phys. Chem. C.* 122 (2018) 5710–5720.
- [30] W.A. Steele, The interaction of gases with solid surfaces, Pergamon (1974).
- [31] A. Wongkoblap, D.D. Do, Adsorption of polar and nonpolar fluids in finite-length carbon slit pore: a Monte Carlo simulation study, *Chem. Eng. Commun.* 195 (2008) 1382–1395.
- [32] D. Do, H. Do, Evaluation of 1-site and 5-site models of methane on its adsorption on graphite and in graphitic slit pores, *J. Phys. Chem. B* 109 (2005) 19288–19295.
- [33] V.S. Kandagal, A. Pathak, K. Ayappa, S.N. Punnathanam, Adsorption on edge-functionalized bilayer graphene nanoribbons: assessing the role of functional groups in methane uptake, *J. Phys. Chem. C.* 116 (2012) 23394–23403.
- [34] Y. Sun, D. Spellmeyer, D.A. Pearlman, P. Kollman, Simulation of the solvation free energies for methane, ethane, and propane and corresponding amino acid dipeptides: a critical test of the bond-PMF correction, a new set of hydrocarbon parameters, and the gas phase-water hydrophobicity scale, *J. Am. Chem. Soc.* 114 (1992) 6798–6801.
- [35] J. Cheng, X. Yuan, L. Zhao, D. Huang, M. Zhao, L. Dai, et al., GCMC simulation of hydrogen physisorption on carbon nanotubes and nanotube arrays, *Carbon* 42 (2004) 2019–2024.
- [36] A.A. Kumar, H. Jobic, S.K. Bhatia, Quantum effects on adsorption and diffusion of hydrogen and deuterium in microporous materials, *J. Phys. Chem. B* 110 (2006) 16666–16671.
- [37] A. Gholidoust, J.D. Atkinson, Z. Hashisho, Enhancing CO₂ adsorption via amine-impregnated activated carbon from oil sands coke, *Energy Fuels* 31 (2017) 1756–1763.
- [38] E. Mehrvarz, A.A. Ghoreyshi, M. Jahanshahi, Surface modification of broom sorghum-based activated carbon via functionalization with triethylenetetramine and urea for CO₂ capture enhancement, *Front. Chem. Sci. Eng.* 11 (2017) 252–265.
- [39] R.S. Rajaura, S. Srivastava, P.K. Sharma, S. Mathur, R. Shrivastava, S. Sharma, et al., Structural and surface modification of carbon nanotubes for enhanced hydrogen storage density, *Nano-Struct. Nano-Objects.* 14 (2018) 57–65.
- [40] Rufford TE, Gao S, Arami-Niya A, Villacorta BS, Ge L, Zhu Z. Methane adsorption on pitch derived activated carbon monoliths. 2018.
- [41] M.E. Casco, M. Martínez-Escandell, K. Kaneko, J. Silvestre-Albero, F. Rodríguez-Reinoso, Very high methane uptake on activated carbons prepared from mesophase pitch: a compromise between microporosity and bulk density, *Carbon* 93 (2015) 11–21.
- [42] M.E. Casco, M. Martínez-Escandell, E. Gadea-Ramos, K. Kaneko, J. Silvestre-Albero, F. Rodríguez-Reinoso, High-pressure methane storage in porous materials: are carbon materials in the pole position? *Chem. Mater.* 27 (2015) 959–964.
- [43] Q. Liu, M. Ke, F. Liu, P. Yu, H. Hu, C. Li, High-performance removal of methyl mercaptan by nitrogen-rich coconut shell activated carbon, *RSC Adv.* 7 (2017) 22892–22899.
- [44] J. Alcañiz-Monge, D. Lozano-Castelló, D. Cazorla-Amorós, A. Linares-Solano, Fundamentals of methane adsorption in microporous carbons, *Microporous Mesoporous Mater.* 124 (2009) 110–116.
- [45] F. Rodríguez-Reinoso, Y. Nakagawa, J. Silvestre-Albero, J. Juárez-Galán, M. Molina-Sabio, Correlation of methane uptake with microporosity and surface area of chemically activated carbons, *Microporous Mesoporous Mater.* 115 (2008) 603–608.
- [46] Y. Gogotsi, C. Portet, S. Osswald, J.M. Simmons, T. Yildirim, G. Laudisio, et al., Importance of pore size in high-pressure hydrogen storage by porous carbons, *Int. J. Hydrogen Energy* 34 (2009) 6314–6319.
- [47] W. Zhao, V. Fierro, C. Zlotea, E. Aylon, M. Izquierdo, M. Lacroche, et al., Activated carbons with appropriate micropore size distribution for hydrogen adsorption, *Int. J. Hydrogen Energy* 36 (2011) 5431–5434.
- [48] H. Boehm, Some aspects of the surface chemistry of carbon blacks and other carbons, *Carbon* 32 (1994) 759–769.
- [49] Schönherr J, Buchheim J, Scholz P, Adelhelm P. Boehm titration revisited (part i): Practical aspects for achieving a high precision in quantifying oxygen-containing surface groups on carbon materials. C. 2018;4:21.
- [50] A. Rehman, S.-J. Park, Comparative study of activation methods to design nitrogen-doped ultra-microporous carbons as efficient contenders for CO₂ capture, *Chem. Eng. J.* 352 (2018) 539–548.
- [51] A. Rehman, S.-J. Park, From chitosan to urea-modified carbons: Tailoring the ultra-microporosity for enhanced CO₂ adsorption, *Carbon* 159 (2020) 625–637.
- [52] D. Lozano-Castello, D. Cazorla-Amorós, A. Linares-Solano, D. Quinn, Influence of pore size distribution on methane storage at relatively low pressure: preparation of activated carbon with optimum pore size, *Carbon* 40 (2002) 989–1002.
- [53] D. Alezi, Y. Belmabkhout, M. Suyetin, P.M. Bhatt, L.J. Weselowski, V. Solovyeva, et al., MOF crystal chemistry paving the way to gas storage needs: aluminum-based soc-MOF for CH₄, O₂, and CO₂ storage, *J. Am. Chem. Soc.* 137 (2015) 13308–13318.
- [54] J.A. Mason, J. Oktawiec, M.K. Taylor, M.R. Hudson, J. Rodriguez, J.E. Bachman, et al., Methane storage in flexible metal-organic frameworks with intrinsic thermal management, *Nature* 527 (2015) 357.
- [55] A. Arami-Niya, T.E. Rufford, Z. Zhu, Nitrogen-doped carbon foams synthesized from banana peel and zinc complex template for adsorption of CO₂, CH₄, and N₂, *Energy Fuels* 30 (2016) 7298–7309.
- [56] Q. Al-Naddaf, M. Al-Mansour, H. Thakkar, F. Rezaei, MOF-GO hybrid nanocomposite adsorbents for methane storage, *Ind. Eng. Chem. Res.* 57 (2018) 17470–17479.
- [57] H. Furukawa, N. Ko, Y.B. Go, N. Aratani, S.B. Choi, E. Choi, et al., Ultrahigh porosity in metal-organic frameworks, *Science* 329 (2010) 424–428.
- [58] A. Arami-Niya, T.E. Rufford, G. Dresch, S. Al Ghafri, F. Jiao, E.F. May, Measurements of helium adsorption on natural clinoptilolite at temperatures from (123.15 to 423.15) K and pressures up to 35 MPa, *Sep. Purif. Technol.* 223 (2019) 1–9.
- [59] C.-C. Huang, H.-M. Chen, C.-H. Chen, J.-C. Huang, Effect of surface oxides on hydrogen storage of activated carbon, *Sep. Purif. Technol.* 70 (2010) 291–295.
- [60] A. Ariharan, B. Viswanathan, V. Nandhakumar, Nitrogen-incorporated carbon nanotube derived from polystyrene and polypyrrole as hydrogen storage material, *Int. J. Hydrogen Energy* 43 (2018) 5077–5088.
- [61] J. Zhao, Z. Wang, P. Guo, Microscopic simulation of methane adsorption in organic matter, *Ind. Eng. Chem. Res.* 58 (2019) 3523–3530.
- [62] P. Ariyagadsakul, V. Vchirawongkwin, C. Kritayakornpong, Determination of toxic carbonyl species including acetone, formaldehyde, and phosgene by poly-aniline emeraldine gas sensor using DFT calculation, *Sens. Actuat. B* 232 (2016) 165–174.
- [63] S. Liu, L. Sun, F. Xu, J. Zhang, C. Jiao, F. Li, et al., Nanosized Cu-MOFs induced by graphene oxide and enhanced gas storage capacity, *Energy Environ. Sci.* 6 (2013) 818–823.
- [64] A.S. Rad, Y.M. Jouibary, V.P. Foukolaei, E. Binaeian, Study on the structure and electronic property of adsorbed guanine on aluminum doped graphene: first principles calculations, *Curr. Appl Phys.* 16 (2016) 527–533.
- [65] D. Klinker Ii, L.J. Broadbelt, A theoretical study of hydrogen chemisorption on Ni (111) and Co (0001) surfaces, *Surf. Sci.* 429 (1999) 169–177.
- [66] J.S. Im, S.-J. Park, Y.-S. Lee, The metal-carbon-fluorine system for improving hydrogen storage by using metal and fluorine with different levels of electro-negativity, *Int. J. Hydrogen Energy* 34 (2009) 1423–1428.
- [67] A. Arami-Niya, T.E. Rufford, G. Birkett, Z. Zhu, Gravimetric adsorption measurements of helium on natural clinoptilolite and synthetic molecular sieves at pressures up to 3500 kPa, *Microporous Mesoporous Mater.* 244 (2017) 218–225.